Inorg. Chem. **2003**, *42*, 1175–1186

The Solid State Structure of $[B_{10}H_{11}]^-$ and Its Dynamic NMR Spectra in Solution

Sheldon G. Shore,*,† Ewan J. M. Hamilton,‡ Adam N. Bridges,† Joseph Bausch,*,§ Jeanette A. Krause-Bauer,† Danan Dou,† Jianping Liu,† Shengming Liu,† Bin Du,† Heather Hall,† Edward A. Meyers,† and Karl E. Vermillion†

Departments of Chemistry, The Ohio State University, Columbus, Ohio 43210, The Ohio State University at Lima, Lima, Ohio 45804, and Villanova University, Villanova, Pennsylvania 19085

Received September 5, 2002

The structure of $[PPh_3(benzyl)][B_{10}H_{11}]$ was determined at –123 °C and 24 °C by single-crystal X-ray analyses. The B_{10} core of $[B_{10}H_{11}]^-$ is similar in shape to that of $[B_{10}H_{10}]^{2-}$. The 11th H atom asymmetrically caps a polar face of the cluster and shows no tendency for disorder in the solid state. Variable temperature multinuclear NMR studies shed light on the dynamic nature of $[B_{10}H_{11}]^-$ in solution. In addition to the fluxionality of the cluster H atoms, the boron cage is fluxional at moderate temperatures, in contrast to $[B_{10}H_{10}]^{2-}$. Multiple exchange processes are believed to take place as a function of temperature. Results of *ab initio* calculations are presented. Crystal data: $[PPh_3(benzyl)][B_{10}H_{11}]$ at –123 °C, $P2_1/c$, $a = 9.988(2)$ Å, $b = 18.860(2)$ Å, $c = 15.072(2)$ Å, $\beta = 107.916(8)°$, $V = 2701.5(7)$ Å^3, $Z = 4$; $[PPh_3(benzyl)][B_{10}H_{11}]$ at 24 °C, $P2_1/c$, $a = 10.067(5)$ Å, $b = 19.009(9)$ Å, $c = 15.247(7)$ Å, $\beta = 107.952(9)°$, $V = 2775(2)$ Å^3, $Z = 4$.

Introduction

The structure of the *closo*-$[B_{10}H_{10}]^{2-}$ anion[1] is that of a bicapped square antiprism with a terminal hydrogen on each boron atom (Chart 1).

Protonation of $[B_{10}H_{10}]^{2-}$ to form $[B_{10}H_{11}]^-$ was first reported in 1973[2] by Wegner, Adams, Callabretta, Spada, and Unger. It is easily prepared[2−4] (eq 1).

$$[B_{10}H_{10}]^{2-} + CF_3CO_2H \rightleftarrows [B_{10}H_{11}]^- + [CF_3CO_2]^- \quad (1)$$

Although the first synthesis of $[B_{10}H_{11}]^-$ was reported 29 years ago,[2] debate continues till the present day as to the exact nature of this species. While its NMR spectra have been reasonably well described,[3,5] they have never been fully understood in terms of relating to a possible structure or structures. At or below room temperature, the $^{11}B\{^1H\}$ NMR spectrum shows only three peaks, with intensity ratio and assignments 1 (B10):5 (B1, B2, B3, B4, B5):4 (B6, B7, B8, B9). The ^{11}B and $^{11}B\{^1H\}$ spectra are shown in Figure 1.

Chart 1. Numbering Scheme for *closo*- B_{10} Structures

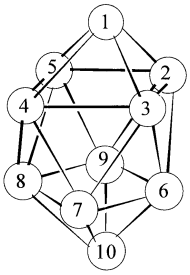

In view of the attachment of the 11th proton, one possibility that has been discussed is that it is involved with the apical boron atom (B1) resulting in a boron resonance that is coincident with that of the four boron atoms that define the upper belt (B2, B3, B4, B5).[6,7]

* Authors to whom correspondence should be addressed. E-mail: shore@chemistry.ohio-state.edu (S.G.S.).
† The Ohio State University.
‡ The Ohio State University at Lima.
§ Villanova University.

(1) Dobrott, R. D.; Lipscomb, W. N. *J. Chem. Phys.* **1962**, *37*, 1779.
(2) Wegner, P. A.; Adams, D. M.; Callabretta, F. G.; Spada, L. T.; Unger, R. G. *J. Am. Chem. Soc*. **1973**, *95*, 7513.
(3) Mustyatsa, V. N.; Votinova, N. A.; Solntsev, K. A.; Kuznetsov, N. T. *Dokl. Chem.* **1988**, *301*, 245. (Originally appeared in Russian as *Dokl. Akad. Nauk. SSSR* **1988**, *301*, 1396.)
(4) Hawthorne, M. F.; Mavunkal, I. J.; Knobler, C. B. *J. Am. Chem. Soc.* **1992**, *114*, 4427.
(5) Mustyatsa, V. N.; Solntsev, K. A.; Sakharov, S. G.; Kuznetsov, N. T. *Dokl. Chem.* **1998**, *358*, 1. (Originally appeared in Russian as *Dokl. Akad. Nauk. SSSR* **1998**, *358*, 68.)

10.1021/ic020540s CCC: $25.00
Published on Web 01/17/2003

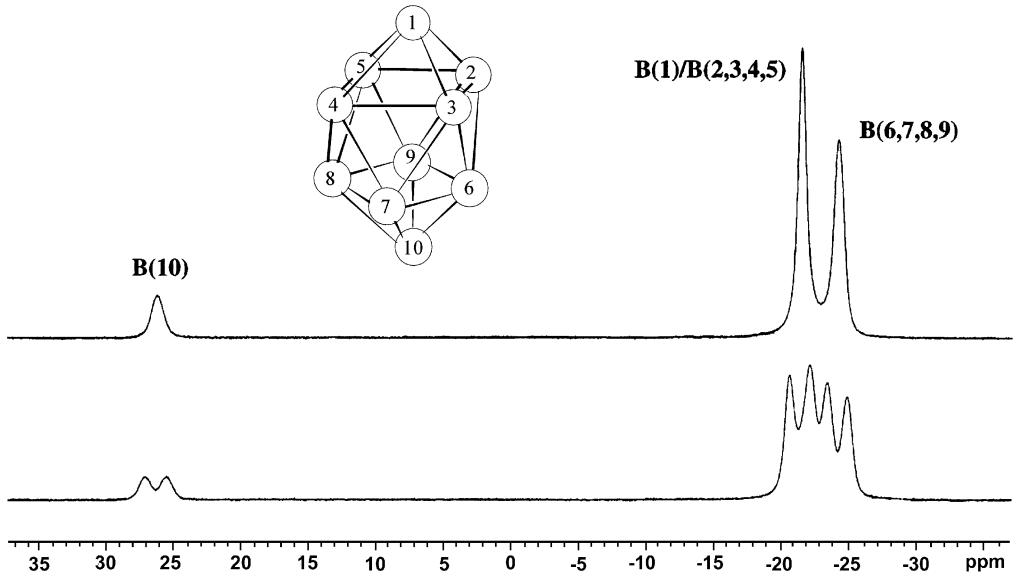

Figure 1. ^{11}B and $^{11}B\{^1H\}$ spectra of $[PPh_4][B_{10}H_{11}]$.

Ab initio calculations have suggested a global energy minimum for $[B_{10}H_{11}]^-$ associated with μ-3 attachment of its 11th H atom, H(*), to a polar face. Migration of H(*) to another apical face (over a B−B connectivity) is associated with only a very small (2.3 kcal/mol) energy barrier, suggesting facile fluxional behavior of H(*). Additionally, a barrier of 8.5 kcal/mol is associated with scrambling of H(1) and H(*) via a BH_2 function. While this facile motion of H(*) would allow the $[B_{10}H_{11}]^-$ anion to possess higher effective symmetry in solution than in the solid state, the appearance of the ^{11}B NMR spectrum, with only three resonances in a 1:5:4 intensity ratio, remains troubling. Another possibility is that the upper half of the anion structure has acquired dynamic character that results in an averaging of the resonances of boron atoms B1−B5.

Previously published structural studies[8,9] of the $[Ph_4P]^+$ and $[Ph_3P(Et)]^+$ salts of $[B_{10}H_{11}]^-$ have not located the position of the 11th H atom associated with the B_{10} cluster, but have suggested that the anion possesses an unusual, partially open structure in the solid state at temperatures above approximately −60 °C. However, at lower temperature the boron framework is much like that of $[B_{10}H_{10}]^{2-}$.[1]

The present report addresses these issues. We have determined the structure of $[PPh_3(benzyl)][B_{10}H_{11}]$ at 24 °C and at −123 °C. Detailed NMR studies coupled with new ab initio calculations shed further light on the fluxional nature of the $[B_{10}H_{11}]^-$ anion.

Furthermore, we have redetermined the $[PPh_3(Et)][B_{10}H_{11}]$ structure. Our new results indicate that it is actually a disordered structure rather than the previously reported partially opened cage architecture.[9] Details of this work are given in the Supporting Information.

Table 1. Crystallographic Data for $[Ph_3P(benzyl)][B_{10}H_{11}]$ at −123 and 24 °C

	at −123 °C	at 24 °C
chem formula	$C_{25}H_{33}B_{10}P$	$C_{25}H_{33}B_{10}P$
fw	472.58	472.58
space group	$P2_1/c$	$P2_1/c$
a, Å	9.988(2)	10.067(5)
b, Å	18.860(2)	19.009(9)
c, Å	15.072(2)	15.247(7)
β, deg	107.916(8)	107.952(9)
vol, Å^3	2701.5(7)	2775(2)
Z	4	4
ρ(calcd), Mg m^{-3}	1.162	1.131
T, °C	−123	24
radiation (λ, Å)	Mo Kα (0.71073)	Mo Kα (0.71073)
μ, mm^{-1}	0.116	0.113
R1[a] [$I > 2\sigma(I)$]	0.0399	0.0565
wR2[b] (all data)	0.1047	0.1550

[a] $R1 = \sum||F_o| - |F_c||/\sum|F_o|$. [b] $wR2 = \{\sum[w(F_o^2 - F_c^2)^2]/\sum[w(F_o^2)^2]\}^{1/2}$.

Results and Discussion

Molecular Structure of $[PPh_3(benzyl)][B_{10}H_{11}]$ at −123 °C and 24 °C. Crystallographic data collected at −123 °C and at 24 °C are summarized in Table 1. Selected distances and angles are listed in Table 2 and Table 3 for the structure at −123 °C and at 24 °C, respectively. Molecular structures of $[PPh_3(benzyl)][B_{10}H_{11}]$ at −123 °C and 24 °C are presented in Figures 2 and 3, respectively.

The 11th hydrogen atom was located and refined in both room temperature and low-temperature structures. These two structures establish the fact that this proton caps the triangular face defined by B1−B2−B3. Careful inspection of difference maps gives no evidence for disorder of this proton.

At −123 °C, the B_{10} cage of $[B_{10}H_{11}]^-$ is similar to that of $[B_{10}H_{10}]^{2-}$.[1] The B−B bond lengths and B−B−B angles in $[B_{10}H_{11}]^-$ are similar to those in $[B_{10}H_{10}]^{2-}$. However the bond lengths between the boron atoms that are capped by the 11th hydrogen are significantly elongated with respect

(6) Mebel, A. M.; Charkin, O. P.; Solntsev, K. A.; Kuznetsov, N. T. *Russ. J. Inorg. Chem.* **1988**, *33*, 1292. (Originally appeared in Russian as *Zh. Neorg. Khim.* **1988**, *33*, 2263.)
(7) Mebel, A. M.; Charkin, O. P.; Bühl, M.; Schleyer, P. v. R. *Inorg. Chem.* **1993**, *32*, 463.
(8) Ponomarev, V. I.; Solntsev, K. A.; Mustyatsa, V. N.; Kuznetsov, N. T. *Koord. Khim.* **1991**, *17*, 640.
(9) Ponomarev, V. I.; Solntsev, K. A.; Mustyatsa, V. N.; Kuznetsov, N. T. *Russ. J. Coord. Chem.* **1992**, *18*, 324. (Originally appeared in Russian as *Koord. Khim.* **1992**, *18*, 372.)

Table 2. Selected Bond Lengths (Å) and Angles (deg) for $[B_{10}H_{11}]^-$ at −123 °C

Bond Lengths

B(1)−B(4)	1.725(2)	B(3)−HB3	1.125(16)	B(8)−B(9)	1.817(2)	B(2)−B(3)	1.983(2)	B(5)−HB5	1.107(18)
B(1)−B(3)	1.786(2)	B(4)−B(8)	1.819(2)	B(9)−B(10)	1.683(3)	B(2)−HB2	1.118(19)	B(6)−B(9)	1.843(2)
B(1)−H(1A)	1.20(3)	B(4)−HB4	1.108(18)	B(10)−HB10	1.10(2)	B(3)−B(4)	1.806(2)	B(6)−HB6	1.087(19)
B(2)−B(5)	1.788(2)	B(5)−B(8)	1.812(2)	B(1)−B(5)	1.730(2)	B(3)−H(1A)	1.40(3)	B(7)−B(8)	1.825(2)
B(2)−B(6)	1.815(3)	B(6)−B(10)	1.713(3)	B(1)−B(2)	1.795(2)	B(4)−B(7)	1.787(2)	B(8)−B(10)	1.709(3)
B(2)−H(1A)	1.54(3)	B(6)−B(7)	1.855(3)	B(1)−HB1	1.10(2)	B(4)−B(5)	1.881(2)	B(8)−HB8	1.106(18)
B(3)−B(7)	1.804(2)	B(7)−B(10)	1.677(3)	B(2)−B(9)	1.805(2)	B(5)−B(9)	1.799(2)	B(9)−HB9	1.135(18)
B(3)−B(6)	1.821(2)	B(7)−HB7	1.127(19)						

Angles

B(4)−B(1)−B(5)	65.97(10)	B(9)−B(5)−B(4)	101.44(10)	B(4)−B(1)−B(3)	61.89(9)	B(2)−B(5)−B(4)	91.94(10)
B(5)−B(1)−B(3)	97.18(11)	B(1)−B(5)−HB5	115.7(9)	B(4)−B(1)−B(2)	97.07(11)	B(8)−B(5)−B(4)	58.99(9)
B(5)−B(1)−B(2)	60.91(9)	B(9)−B(5)−HB5	121.4(9)	B(3)−B(1)−B(2)	67.22(10)	B(2)−B(5)−HB5	131.0(9)
B(4)−B(1)−H(1A)	113.4(13)	B(4)−B(5)−HB5	129.4(9)	B(5)−B(1)−H(1A)	118.1(13)	B(8)−B(5)−HB5	119.0(9)
B(3)−B(1)−H(1A)	51.5(13)	B(10)−B(6)−B(3)	111.15(12)	B(2)−B(1)−H(1A)	57.8(13)	B(10)−B(6)−B(2)	111.53(12)
B(4)−B(1)−HB1	130.1(10)	B(10)−B(6)−B(9)	56.34(10)	B(5)−B(1)−HB1	127.9(10)	B(2)−B(6)−B(3)	66.08(9)
B(3)−B(1)−HB1	134.9(10)	B(3)−B(6)−B(9)	104.63(11)	B(2)−B(1)−HB1	132.5(10)	B(2)−B(6)−B(9)	59.11(9)
H(1A)−B(1)−HB1	100.2(16)	B(2)−B(6)−B(7)	103.89(11)	B(5)−B(2)−B(1)	57.73(9)	B(10)−B(6)−B(7)	55.87(10)
B(5)−B(2)−B(9)	60.11(9)	B(9)−B(6)−B(7)	88.72(10)	B(1)−B(2)−B(9)	112.47(11)	B(3)−B(6)−B(7)	58.74(9)
B(5)−B(2)−B(6)	102.10(11)	B(2)−B(6)−HB6	120.8(10)	B(1)−B(2)−B(6)	109.76(11)	B(10)B(6)−HB6	118.8(10)
B(9)−B(2)−B(6)	61.24(10)	B(9)−B(6)−HB6	133.6(10)	B(5)−B(2)−B(3)	88.61(9)	B(3)−B(6)−HB6	117.3(10)
B(1)−B(2)−B(3)	56.17(8)	B(10)−B(7)−B(4)	113.86(12)	B(9)−B(2)−B(3)	99.86(10)	B(7)−B(6)−HB6	129.1(10)
B(6)−B(2)−B(3)	57.12(9)	B(4)−B(7)−B(3)	60.41(9)	B(5)−B(2)−H(1A)	98.6(10)	B(10)−B(7)−B(3)	113.80(13)
B(1)−B(2)−H(1A)	41.3(10)	B(4)−B(7)−B(8)	60.47(9)	B(9)−B(2)−H(1A)	141.7(10)	B(10)−B(7)−B(8)	58.23(10)
B(6)−B(2)−H(1A)	97.5(10)	B(10)−B(7)−B(6)	57.77(10)	B(3)−B(2)−H(1A)	44.7(10)	B(3)−B(7)−B(8)	103.48(11)
B(5)−B(2)−HB2	133.9(10)	B(3)−B(7)−B(6)	59.69(9)	B(1)−B(2)−HB2	118.9(10)	B(4)−B(7)−B(6)	101.09(11)
B(9)−B(2)−HB2	122.0(10)	B(10)−B(7)−HB7	122.3(10)	B(6)−B(2)−HB2	119.0(10)	B(8)−B(7)−B(6)	90.04(10)
B(3)−B(2)−HB2	130.1(10)	B(3)−B(7)−HB7	115.0(10)	H(1A)−B(2)−HB2	95.9(14)	B(4)−B(7)−HB7	115.9(10)
B(1)−B(3)−B(7)	111.68(11)	B(6)−B(7)−HB7	133.3(10)	B(1)−B(3)−B(4)	57.38(9)	B(8)−B(7)−HB7	132.1(10)
B(7)−B(3)−B(4)	59.33(9)	B(10)−B(8)−B(9)	56.92(10)	B(1)−B(3)−B(6)	109.86(11)	B(10)−B(8)−B(5)	111.29(12)
B(7)−B(3)−B(6)	61.57(10)	B(10)−B(8)−B(4)	110.71(12)	B(4)−B(3)−B(6)	101.66(11)	B(5)−B(8)−B(9)	59.43(9)
B(1)−B(3)−B(2)	56.61(9)	B(9)−B(8)−B(4)	103.15(11)	B(7)−B(3)−B(2)	99.40(10)	B(5)−B(8)−B(4)	62.39(9)
B(4)−B(3)−B(2)	88.14(9)	B(5)−B(8)−B(7)	102.45(11)	B(6)−B(3)−B(2)	56.79(9)	B(10)−B(8)−B(7)	56.53(10)
B(1)−B(3)−H(1A)	42.1(11)	B(4)−B(8)−B(7)	58.72(9)	B(7)−B(3)−H(1A)	146.1(11)	B(9)−B(8)−B(7)	90.47(11)
B(4)−B(3)−H(1A)	99.5(11)	B(5)−B(8)−HB8	118.0(9)	B(6)−B(3)−H(1A)	102.5(11)	B(10)−B(8)−HB8	121.6(9)
B(2)−B(3)−H(1A)	50.6(11)	B(4)−B(8)−HB8	118.5(9)	B(1)−B(3)−HB3	120.9(8)	B(9)−B(8)−HB8	131.0(9)
B(7)−B(3)−HB3	121.3(8)	B(10)−B(9)−B(5)	113.17(12)	B(4)−B(3)−HB3	136.0(8)	B(7)−B(8)−HB8	132.2(9)
B(6)−B(3)−HB3	116.8(8)	B(5)−B(9)−B(2)	59.48(9)	B(2)−B(3)−HB3	130.0(8)	B(10)−B(9)−B(2)	113.50(12)
H(1A)−B(3)−HB3	92.5(14)	B(5)−B(9)−B(8)	60.14(9)	B(1)−B(4)−B(7)	115.54(12)	B(10)−B(9)−B(8)	58.29(10)
B(1)−B(4)−B(3)	60.72(9)	B(10)−B(9)−B(6)	57.93(10)	B(7)−B(4)−B(3)	60.26(9)	B(2)−B(9)−B(8)	102.97(11)
B(1)−B(4)−B(8)	112.64(11)	B(2)−B(9)−B(6)	59.65(9)	B(7)−B(4)−B(8)	60.81(9)	B(5)−B(9)−B(6)	100.55(10)
B(3)−B(4)−B(8)	103.62(11)	B(10)−B(9)−HB9	122.4(9)	B(1)−B(4)−B(5)	57.14(9)	B(8)−B(9)−B(6)	90.67(10)
B(7)−B(4)−B(5)	101.25(11)	B(2)−B(9)−HB9	114.8(9)	B(3)−B(4)−B(5)	91.30(10)	B(5)−B(9)−HB9	117.4(9)
B(8)−B(4)−B(5)	58.62(8)	B(6)−B(9)−HB9	131.7(9)	B(1)−B(4)−HB4	115.5(10)	B(8)−B(9)−HB9	133.2(9)
B(7)−B(4)−HB4	120.9(9)	B(7)−B(10)−B(8)	65.24(11)	B(3)−B(4)−HB4	129.8(9)	B(7)−B(10)−B(9)	100.67(12)
B(8)−B(4)−HB4	120.3(9)	B(7)−B(10)−B(6)	66.36(11)	B(5)−B(4)−HB4	130.9(9)	B(9)−B(10)−B(8)	64.80(10)
B(1)−B(5)−B(2)	61.36(9)	B(8)−B(10)−B(6)	99.07(12)	B(1)−B(5)−B(9)	115.99(12)	B(9)−B(10)−B(6)	65.73(11)
B(2)−B(5)−B(9)	60.41(9)	B(9)−B(10)−HB10	129.8(11)	B(1)−B(5)−B(8)	112.74(11)	B(7)−B(10)−HB10	129.5(11)
B(2)−B(5)−B(8)	103.86(11)	B(6)−B(10)−HB10	130.1(11)	B(9)−B(5)−B(8)	60.43(9)	B(8)−B(10)−HB10	130.8(11)
B(1)−B(5)−B(4)	56.89(9)						

to the other B−B connectivities in the cluster: B1−B2 (1.795(2) Å); B1−B3 (1.786(2) Å); B2−B3 (1.983(2) Å). In contrast, the bond lengths between the other apical boron, B10, and the equatorial boron atoms (B6, B7, B8, and B9) range from 1.677(3) Å to 1.713(3) Å and are in reasonable agreement with those found in $[B_{10}H_{10}]^{2-}$ (1.70 Å). The B2−B3 separation (at the base of the capped face) is 0.1 Å longer than any other B−B distance in the anion. These structural results are fully consistent with the lowest energy configuration predicted by the earlier theoretical studies,[6,7] including the predicted significant lengthening of B2−B3. Using the same crystal, five additional X-ray data sets were collected in the temperature range from −93 °C to 24 °C. The principal change in the structures determined throughout the entire temperature range is that the thermal parameters increase with increasing temperature as shown in Figures 2 and 3. There is no evidence for disorder of the 11th proton in these structures. This crucial finding distinguishes the present work from previous structural determinations of $[B_{10}H_{11}]^-$salts.[8,9]

Structural Studies on $[Ph_4P][B_{10}H_{11}]$ and $[Ph_3P(Et)][B_{10}H_{11}]$. Structural studies of $[Ph_4P][B_{10}H_{11}]$ and $[Ph_3P(Et)][B_{10}H_{11}]$ were performed previously.[8,9] These determinations were carried out at 27 °C for the former salt and at 27 °C and −163 °C for the latter. The 11th H atom associated with the cage could not be located in any of that work. As part of the present detailed investigation of the $[B_{10}H_{11}]^-$ ion, these structures were redetermined.

The structure of $[Ph_4P][B_{10}H_{11}]$ was investigated at −150 °C and 24 °C. Both studies confirmed the previous report[8] of disorder in the crystal. The structure of $[Ph_3P(Et)][B_{10}H_{11}]$

Table 3. Bond Lengths (Å) and Angles (deg) for $[B_{10}H_{11}]^-$ at 24 °C

Bond Lengths

B(1)−B(4)	1.716(4)	B(3)−HB3	1.12(3)	B(8)−B(9)	1.795(4)	B(2)−B(3)	1.930(4)	B(5)−HB5	1.10(3)
B(1)−B(3)	1.741(5)	B(4)−B(8)	1.799(4)	B(9)−B(10)	1.651(5)	B(2)−HB2	1.10(3)	B(6)−B(9)	1.806(4)
B(1)−H(1A)	1.07(9)	B(4)−HB4	1.11(3)	B(10)−HB10	1.19(4)	B(3)−B(6)	1.772(4)	B(6)−HB6	1.05(3)
B(2)−B(5)	1.789(4)	B(5)−B(9)	1.800(4)	B(1)−B(5)	1.722(4)	B(3)−H(1A)	1.15(9)	B(7)−B(8)	1.831(5)
B(2)−B(6)	1.791(5)	B(6)−B(10)	1.698(5)	B(1)−B(2)	1.757(5)	B(4)−B(7)	1.759(4)	B(8)−B(10)	1.660(5)
B(2)−H(1A)	1.55(9)	B(6)−B(7)	1.831(5)	B(1)−HB1	1.12(4)	B(4)−B(5)	1.850(4)	B(8)−HB8	1.11(3)
B(3)−B(7)	1.760(5)	B(7)−B(10)	1.643(5)	B(2)−B(9)	1.794(4)	B(5)−B(8)	1.792(4)	B(9)−HB9	1.13(3)
B(3)−B(4)	1.824(4)	B(7)−HB7	1.15(3)						

Angles

B(4)−B(1)−B(5)	65.08(18)	B(8)−B(5)−B(4)	59.19(16)	B(4)−B(1)−B(3)	63.68(19)	B(2)−B(5)−B(4)	92.15(18)
B(5)−B(1)−B(3)	97.7(2)	B(1)−B(5)−HB5	117.8(15)	B(4)−B(1)−B(2)	98.0(2)	B(9)−B(5)−B(4)	100.88(19)
B(5)−B(1)−B(2)	61.90(19)	B(8)−B(5)−HB5	119.9(14)	B(3)−B(1)−B(2)	67.0(2)	B(2)−B(5)−HB5	128.4(14)
B(4)−B(1)−H(1A)	103(5)	B(4)−B(5)−HB5	132.5(14)	B(5)−B(1)−H(1A)	119(5)	B(9)−B(5)−HB5	119.5(15)
B(3)−B(1)−H(1A)	40(5)	B(10)−B(6)−B(2)	111.5(2)	B(2)−B(1)−H(1A)	61(5)	B(10)−B(6)−B(3)	110.2(2)
B(4)−B(1)−HB1	129.1(19)	B(10)−B(6)−B(9)	56.14(18)	B(5)−B(1)−HB1	130.9(19)	B(3)−B(6)−B(2)	65.59(19)
B(3)−B(1)−HB1	131.4(19)	B(2)−B(6)−B(9)	59.86(18)	B(2)−B(1)−HB1	132.9(19)	B(3)−B(6)−B(9)	105.0(2)
H(1A)−B(1)−HB1	104(5)	B(3)−B(6)−B(7)	58.44(18)	B(1)−B(2)−B(5)	58.10(17)	B(10)−B(6)−B(7)	55.3(2)
B(1)−B(2)−B(9)	112.6(2)	B(9)−B(6)−B(7)	89.0(2)	B(5)−B(2)−B(9)	60.28(16)	B(2)−B(6)−B(7)	103.6(2)
B(1)−B(2)−B(6)	109.3(2)	B(3)−B(6)−HB6	116.8(15)	B(5)−B(2)−B(6)	101.9(2)	B(10)−B(6)−HB6	124.1(16)
B(9)−B(2)−B(6)	60.49(18)	B(9)−B(6)−HB6	130.5(15)	B(1)−B(2)−B(3)	56.13(18)	B(2)−B(6)−HB6	114.4(16)
B(5)−B(2)−B(3)	88.92(17)	B(10)−B(7)−B(4)	112.7(2)	B(9)−B(2)−B(3)	99.2(2)	B(7)−B(6)−HB6	134.9(16)
B(6)−B(2)−B(3)	56.75(16)	B(4)−B(7)−B(3)	62.45(18)	B(1)−B(2)−H(1A)	37(3)	B(10)−B(7)−B(3)	113.5(3)
B(5)−B(2)−H(1A)	93(3)	B(4)−B(7)−B(8)	60.11(17)	B(9)−B(2)−H(1A)	132(3)	B(10)−B(7)−B(8)	56.8(2)
B(6)−B(2)−H(1A)	91(4)	B(10)−B(7)−B(6)	58.2(2)	B(3)−B(2)−H(1A)	36(4)	B(3)−B(7)−B(8)	104.0(2)
B(1)−B(2)−HB2	118.9(15)	B(3)−B(7)−B(6)	59.10(18)	B(5)−B(2)−HB2	132.3(16)	B(4)−B(7)−B(6)	102.1(2)
B(9)−B(2)−HB2	121.6(15)	B(10)−B(7)−HB7	124.8(16)	B(6)−B(2)−HB2	120.4(16)	B(8)−B(7)−B(6)	89.8(2)
B(3)−B(2)−HB2	131.5(15)	B(3)−B(7)−HB7	113.1(16)	H(1A)−B(2)−HB2	106(3)	B(4)−B(7)−HB7	114.0(16)
B(1)−B(3)−B(7)	111.8(2)	B(6)−B(7)−HB7	133.3(16)	B(1)−B(3)−B(6)	110.9(2)	B(8)−B(7)−HB7	133.2(16)
B(7)−B(3)−B(6)	62.5(2)	B(10)−B(8)−B(9)	56.9(2)	B(1)−B(3)−B(4)	57.50(17)	B(10)−B(8)−B(5)	111.8(2)
B(7)−B(3)−B(4)	58.74(18)	B(10)−B(8)−B(4)	109.9(2)	B(6)−B(3)−B(4)	101.9(2)	B(5)−B(8)−B(9)	60.23(17)
B(1)−B(3)−B(2)	56.90(18)	B(9)−B(8)−B(4)	103.05(19)	B(7)−B(3)−B(2)	100.8(2)	B(5)−B(8)−B(4)	62.00(16)
B(6)−B(3)−B(2)	57.66(18)	B(5)−B(8)−B(7)	101.2(2)	B(4)−B(3)−B(2)	88.53(18)	B(10)−B(8)−B(7)	55.9(2)
B(1)−B(3)−H(1A)	37(4)	B(4)−B(8)−B(7)	57.96(18)	B(7)−B(3)−H(1A)	145(4)	B(9)−B(8)−B(7)	89.3(2)
B(6)−B(3)−H(1A)	108(4)	B(5)−B(8)−HB8	120.3(16)	B(4)−B(3)−H(1A)	94(4)	B(10)−B(8)−HB8	120.8(16)
B(2)−B(3)−H(1A)	53(4)	B(4)−B(8)−HB8	117.9(15)	B(1)−B(3)−HB3	118.7(13)	B(9)−B(8)−HB8	133.3(15)
B(7)−B(3)−HB3	120.6(13)	B(10)−B(9)−B(2)	113.5(2)	B(6)−B(3)−HB3	119.9(13)	B(7)−B(8)−HB8	130.4(15)
B(4)−B(3)−HB3	132.4(13)	B(2)−B(9)−B(8)	103.45(19)	B(2)−B(3)−HB3	131.9(13)	B(10)−B(9)−B(8)	57.4(2)
H(1A)−B(3)−HB3	94(4)	B(2)−B(9)−B(5)	59.72(17)	B(1)−B(4)−B(7)	113.1(2)	B(10)−B(9)−B(5)	111.8(2)
B(1)−B(4)−B(8)	112.7(2)	B(10)−B(9)−B(6)	58.6(2)	B(7)−B(4)−B(8)	61.93(19)	B(8)−B(9)−B(5)	59.82(16)
B(1)−B(4)−B(3)	58.82(19)	B(8)−B(9)−B(6)	91.8(2)	B(7)−B(4)−B(3)	58.80(18)	B(2)−B(9)−B(6)	59.65(18)
B(8)−B(4)−B(3)	102.73(19)	B(10)−B(9)−HB9	122.0(15)	B(1)−B(4)−B(5)	57.61(17)	B(5)−B(9)−B(6)	100.88(19)
B(7)−B(4)−B(5)	101.8(2)	B(8)−B(9)−HB9	133.4(14)	B(8)−B(4)−B(5)	58.82(16)	B(2)−B(9)−HB9	114.9(15)
B(3)−B(4)−B(5)	90.40(17)	B(6)−B(9)−HB9	129.7(14)	B(1)−B(4)−HB4	114.6(14)	B(5)−B(9)−HB9	119.1(15)
B(7)−B(4)−HB4	124.5(14)	B(7)−B(10)−B(8)	67.3(2)	B(8)−B(4)−HB4	119.6(14)	B(7)−B(10)−B(9)	101.4(2)
B(3)−B(4)−HB4	133.3(13)	B(7)−B(10)−B(6)	66.5(2)	B(5)−B(4)−HB4	127.1(13)	B(9)−B(10)−B(8)	65.63(19)
B(1)−B(5)−B(2)	60.00(18)	B(8)−B(10)−B(6)	100.7(2)	B(1)−B(5)−B(8)	112.7(2)	B(9)−B(10)−B(6)	65.2(2)
B(2)−B(5)−B(8)	103.8(2)	B(9)−B(10)−HB10	130.6(18)	B(1)−B(5)−B(9)	114.0(2)	B(7)−B(10)−HB10	128.0(18)
B(2)−B(5)−B(9)	60.00(17)	B(6)−B(10)−HB10	129.0(18)	B(8)−B(5)−B(9)	59.96(16)	B(8)−B(10)−HB10	130.4(18)
B(1)−B(5)−B(4)	57.31(17)						

was determined at −80 °C and −40 °C since a phase transformation in the crystal was reported earlier[9] and this result was confirmed.

In our work on these compounds the 11th hydrogen could not be unambiguously located and all of the structures appeared to be disordered in some way. Experimental details regarding them are given in the Supporting Information.

These observations suggest that the degree of disorder both in the boron atom framework and in the position of the 11th H atom in the $[B_{10}H_{11}]^-$ ion is dependent on the particular cation present.

A related system for which a reasonable quantity of prior experimental and theoretical data exists is $[B_6H_6]^{2-}/[B_6H_7]^-$. This system is similar to that of $[B_{10}H_{10}]^{2-}/[B_{10}H_{11}]^-$ in that protonation of a closo polyhedron leads to a moderately stable fluxional monoanion. However, they also differ in significant ways. $[B_6H_6]^{2-}$ possesses an octahedral structure. All six boron atoms in the cluster are connected to four other equivalent borons. The high symmetry of this ion offers only very limited choices of sites in which to place an additional proton.

X-ray structural determinations of $[Ph_4P]^+$ and $[Ni(bipy)_3]^{2+}$ salts of $[B_6H_7]^-$ suffer from problems due to disorder in the anions, as in the case of $[B_{10}H_{11}]^-$, but when the $[Ni(phen)_3]^{2+}$ cation was employed there was no anion disorder and the seventh proton was found bonded to the polyhedron in a face-capping arrangement.[10] Protonation leads to clear distortions of the closo architecture with respect

(10) Kuznetsov, I. Yu.; Vinitskii, D. M.; Solntsev, K. A.; Kuznetsov, N. T.; Butman, L. A. *Dokl. Akad. Nauk. SSSR* **1985**, *283*, 873.

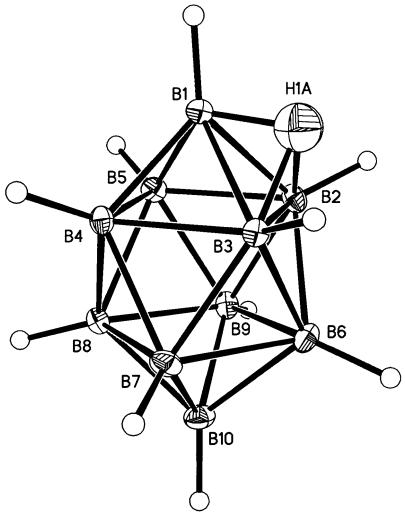

Figure 2. Plot of $[B_{10}H_{11}]^-$ at −123 °C (25% probability ellipsoids for boron and H1A).

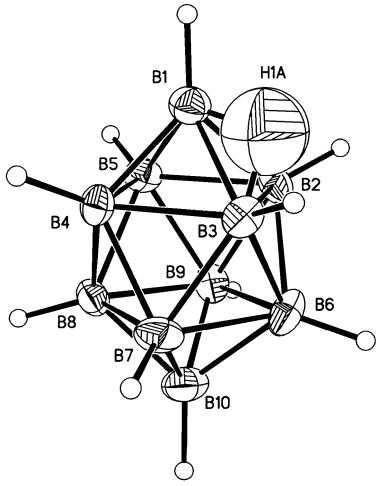

Figure 3. Plot of $[B_{10}H_{11}]^-$ at 24 °C (25% probability ellipsoids for boron and H1A).

to that of the parent $[B_6H_6]^{2-}$ cluster. B−B distances within the capped face are markedly longer (≈1.8 Å) than those involving boron atoms not associated with the additional proton (≈1.7 Å). Additionally, NMR studies show $[B_6H_7]^-$ to be fluxional in solution at or above room temperature, with the seventh proton migrating from face to face of the closo polyhedron,[11] consistent with theoretical considerations.[12] However, this dynamic behavior can be arrested at −80 °C, where 2 doublets of equal intensity are observed in the ^{11}B spectrum, one signal corresponding to the three boron atoms of the capped face, and the other to the boron atoms which are not associated with the nonterminal H.

Table 4. T1 Values Obtained from Fitting the Peak Intensities in the ^{11}B NMR Spectrum of $[Ph_4P][B_{10}H_{11}]$

assignment	frequency (Hz)	ppm	T1 (ms)
B(10)	4076, −3931	−25.4, −24.5	24.1, 24.1
B(1), B(2−5)	−3616, −3483	−22.5, −21.7	24.5, 25.0
B(6−9)	4007, 4151	25.0, 25.9	34.8, 33.4

NMR Studies of $[PPh_4][B_{10}H_{11}]$. As shown in Figure 1, the $^{11}B\{^1H\}$ spectrum of $[PPh_4][B_{10}H_{11}]$ recorded at room temperature shows three signals in a 1:5:4 intensity ratio, as previously reported.[3,5] All signals appear as doublets in the ^{11}B spectrum. The spectrum appears consistent with an 11th H atom which is highly fluxional in nature, associated with only one apical region of the cluster. All resonances have been assigned by a $^{11}B\{^1H\}-^{11}B\{^1H\}$ COSY experiment, assuming the highest frequency resonance to correspond to B(10). The signal of intensity 5 corresponds to B(1) and B(2−5) and is not resolved into more than one component even at high fields (Bruker DRX-500 spectrometer operating at a boron resonance frequency of 160.1 MHz). Partial relaxation experiments performed using the inversion recovery pulse sequence[13] were unable to discern any differences in T1 relaxation times of the B(1) and B(2−5) resonances. T1 values obtained from fitting the peak intensities in the ^{11}B NMR spectrum are shown in Table 4. These data show no significant differences within each doublet, and offer no evidence for accidental overlap of the B(1) and B(2−5) signals. This suggests that the signal of relative intensity 5 arises as a result of magnetic equivalence, rather than accidental overlap.

Theoretical calculations of the chemical shifts using GIAO theory at the B3LYP/6-311G* level (see below) suggest that magnetic equivalence is plausible. It is reasonable to average the B(2)−B(5) shifts, as these signals are rendered equivalent in solution on the ^{11}B NMR time scale at room temperature as a result of the rapid fluxionality of the additional proton around the polar region of the cluster. Calculated shifts (ppm) are as follows: B(1), −25.2, and B(2)−B(5) (average), −18.9. The weighted average of these two values provides a value of −20.1 ppm. This theoretical value compares reasonably well with the position of the observed signal of relative intensity 5 in the $^{11}B\{^1H\}$ spectrum that appears at −21.7 ppm.

Thus an exchange process is suggested by which vertices B(1)−B(5) become equivalent on the ^{11}B NMR time scale. The lengthening of B−B connectivities observed in the solid state, associated with the asymmetric μ-3 attachment of the 11th H atom to a cluster face, might be reasonably viewed as an initial step in a sequence of bond rupture and re-formation processes permitting fluxional behavior of the borane skeleton. No noticeable changes are observed in the $^{11}B\{^1H\}$ spectrum upon lowering the temperature as low as

(11) (a) Vinitskii, D. M.; Lagun, V. L.; Solntsev, K. A.; Kuznetsov, N. T.; Kuznetsov, I. Yu. *Koord. Khim.* **1985**, *11*, 1504. (b) Solntsev, K. A.; Buslaev, Yu. A.; Kuznetsov, N. T. *Russ. J. Inorg. Chem.* **1986**, *31*, 633. (Originally appeared in Russian as *Zh. Neorg. Khim.* **1986**, *31*, 1113.) (c) Panyushkin, V. T.; Vaschuk, A. V.; Tarasov, V. P. *J. Struct. Chem.* **1992**, *33*, 388. (Originally appeared in Russian as *Zh. Strukt. Khim.* **1992**, *33*, 65.)

(12) (a) Mebel, A. M.; Charkin, O. P.; Kuznetsov, I. Yu.; Solntsev, K. A.; Kuznetsov, N. T. *Russ. J. Inorg. Chem.* **1988**, *33*, 958. (Originally appeared in Russian as *Zh. Neorg. Khim.* **1988**, *33*, 1685.) (b) Mebel, A. M.; Charkin, O. P. *J. Struct. Chem.* **1989**, *30*, 173. (Originally appeared in Russian as *Zh. Strukt. Khim.* **1989**, *30*, 7.) (c) Kuznetsov, I. Yu.; Solntsev, K. A.; Kuznetsov, N. T. *Dokl. Phys. Chem.* **1987**, *295*, 639. (Originally appeared in Russian as *Dokl. Akad. Nauk. SSSR* **1987**, *295*, 138.) (d) McKee, M. L.; Bühl, M.; Charkin, O. P.; Schleyer, P. v. R. *Inorg. Chem.* **1993**, *32*, 4549.

(13) Braun, S.; Kalinowski, H.-O.; Berger, S. *150 and More Basic NMR Experiments: A Practical Course*, 2nd expanded ed.; Wiley-VCH: Weinheim, 1998; pp 155−158.

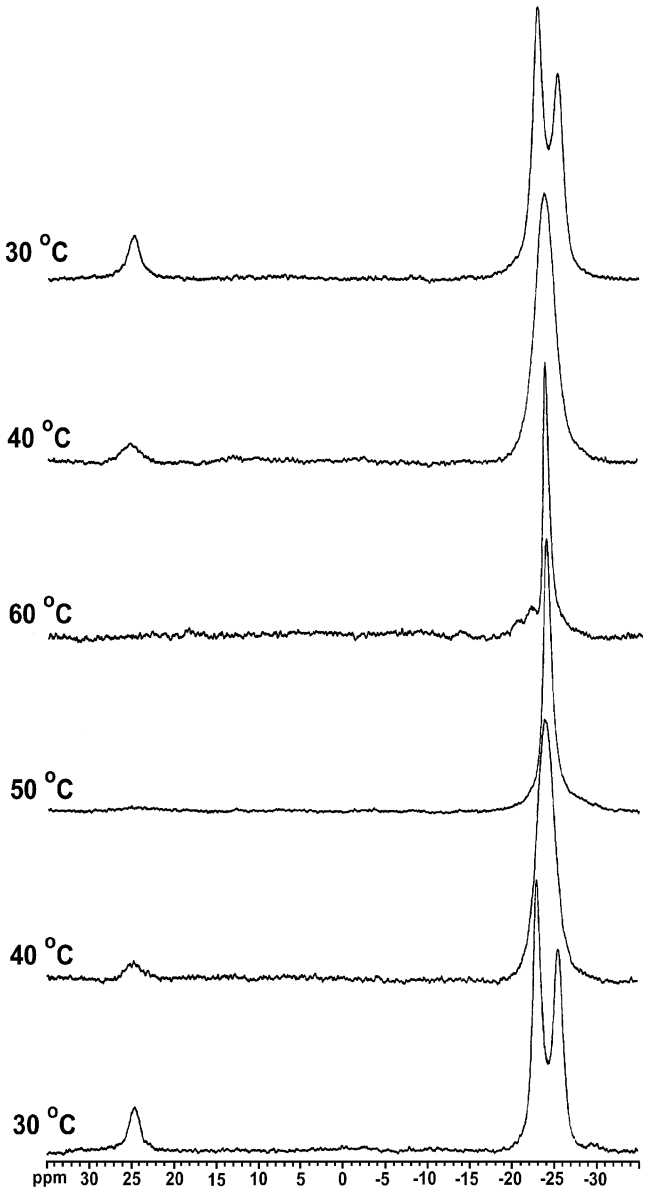

Figure 4. High-temperature $^{11}B\{^1H\}$ spectra of $[PPh_4][B_{10}H_{11}]$.

−70 °C. Even at −90 °C, the spectrum shows only the expected quadrupolar broadening.

Evidence was obtained for the fluxionality of the B_{10} cage of $[B_{10}H_{11}]^-$, a property that we did not observe in the case of $[B_{10}H_{10}]^{2-}$. In the $^{11}B\{^1H\}$ spectrum of $[B_{10}H_{11}]^-$ at 60 °C the signals at −21.7 ppm (intensity 5) and −24.3 ppm (intensity 4) are coalesced into a relatively sharp single peak centered around the weighted average of the two original signals, while the B(10) signal is broadened into the baseline at this temperature, and does not apparently contribute to the chemical shift of the new signal.

Thus, the suggestion is that the barrier to inclusion of the next belt of boron atoms B(6−9) in the fluxional process is overcome by 60 °C. As shown in Figure 4, this effect is completely reversible on returning the temperature to 30 °C.

Further evidence for vertex exchange in $[B_{10}H_{11}]^-$ may be taken from a room temperature $^{11}B\{^1H\}-^{11}B\{^1H\}$ NOESY/EXSY experiment.[14,15] The NOESY/EXSY spectrum of $[PPh_4][B_{10}H_{11}]$ is shown in Figure 5.

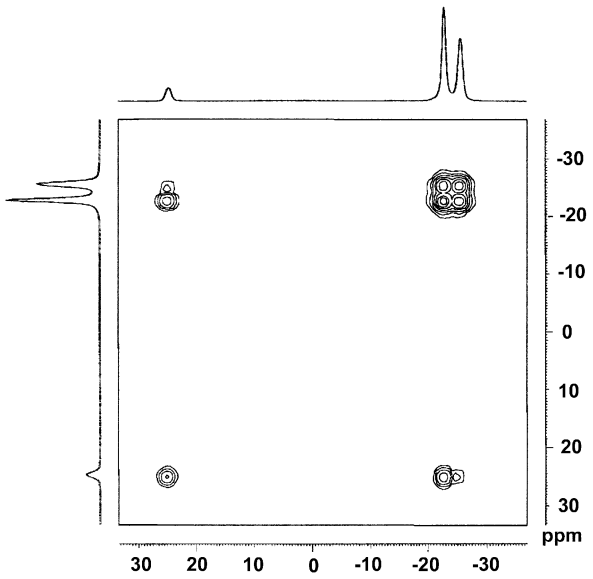

Figure 5. NOESY/EXSY plot of $[PPh_4][B_{10}H_{11}]$ at room temperature.

The mixing time was 50 ms. The spectrum is phased such that the diagonal peaks are positive, and only positive contours are shown. The strong off-diagonal peaks of the same phase as the diagonal peaks are indicative of chemical exchange in small, rapidly tumbling molecules such as $[B_{10}H_{11}]^-$. Spectra obtained with 10 ms mixing time showed similar features. At lower temperature (−40 °C), the cross peaks in the $[PPh_4][B_{10}H_{11}]$ NOESY/EXSY spectrum also disappeared, indicating the exchange process to be either arrested or slower than the chosen delay at this temperature. As a control, the NOESY/EXSY experiment was conducted on $[PPh_4]_2[B_{10}H_{10}]$. A mixing time of 10 ms gave a better signal-to-noise ratio than 50 ms. No positive off-diagonal peaks were observed, indicating that no chemical exchange is occurring in $[B_{10}H_{10}]^{2-}$ on the order of the mixing time.

$^1H\{^{11}B\}$ spectra of $[PPh_4][B_{10}H_{11}]$ at a range of temperatures from −90 °C to 10 °C are shown in Figure 6. The signals from H(1) and the extra hydrogen, H(*), are seen to diminish as temperature is raised, and are replaced by a signal of intermediate chemical shift.

The $^1H\{^{11}B\}$ spectra of $[PPh_4][B_{10}H_{11}]$ at −90 °C and at 0 °C are shown in Figure 7.

The $^1H\{^{11}B\}$ spectrum at −90 °C shows 5 signals in relative intensities 1:1:4:4:1. The resonance at 4.99 ppm was identified as H(10) by selective decoupling. The two signals of intensity 4 (1.03 and 0.55 ppm) are attributed to terminal H atoms associated with the equatorial belts of the cluster. The remaining signals are assigned to H(*) (−1.80 ppm) and H(1) (3.03 ppm) by reference to theoretically calculated values. Specifically, calculated ^1H chemical shifts are as follows: H(1) 3.1 ppm and H(*) −2.4 ppm. The difference between these values is 5.5 ppm, compared to an experimentally observed difference of around 4.8 ppm between the two resonances. At 0 °C, the H(1) and H(*) signals are replaced by a signal of relative intensity 2 at an intermediate

(14) Jeener, J.; Meier, B. H.; Bachmann, P.; Ernst, R. R. *J. Chem. Phys.* **1979**, *71*, 4546−4553.
(15) Wagner, R.; Berger, S. *J. Magn. Reson. A.* **1996**, *123*, 229−232.

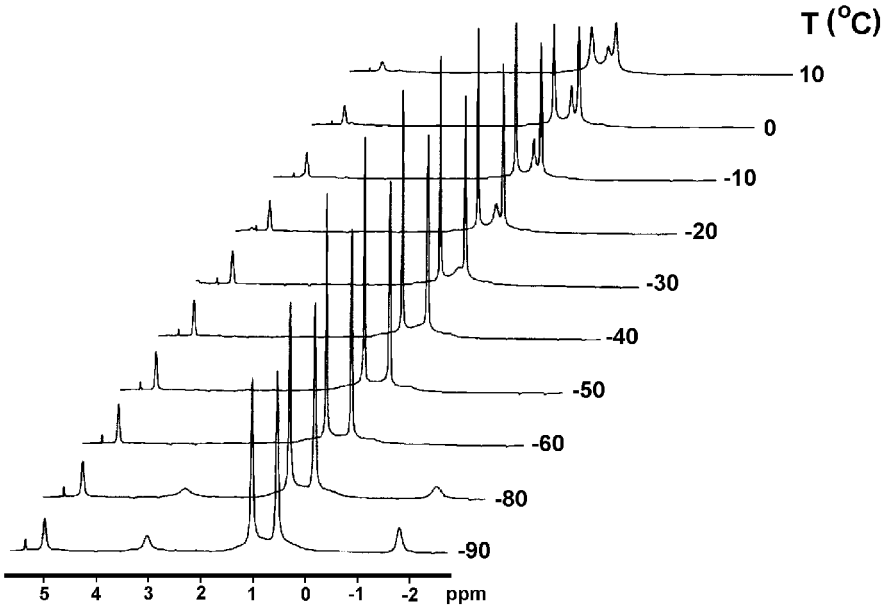

Figure 6. Stacked plots showing changes in $^1H\{^{11}B\}$ spectra of $[PPh_4][B_{10}H_{11}]$ from −90 to 10 °C.

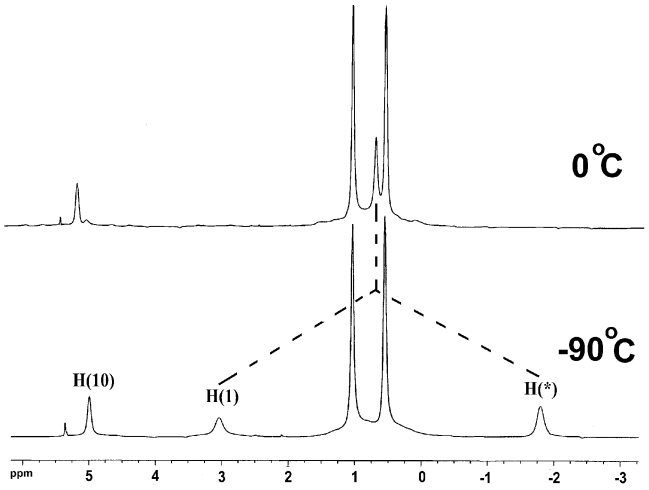

Figure 7. $^1H\{^{11}B\}$ spectra of $[PPh_4][B_{10}H_{11}]$ at −90 and 0 °C.

chemical shift of 0.78 ppm. (The average of the calculated values would appear at −0.35 ppm.) This is suggestive of an exchange process between H(1) and H(*) at this temperature, in accord with earlier theoretical predictions of a low barrier to exchange via a $\{BH_2\}$ function.[6,7] This barrier would appear to be surmounted at 0 °C, but not at −90 °C.

At temperatures above 0 °C the behavior of the $^1H\{^{11}B\}$ spectrum parallels that of the $^{11}B\{^1H\}$ spectrum. As the temperature increases, the cage proton signals begin to coalesce. By 40 °C, there remains only a single, broad peak associated with the protons of the anion. The peak further sharpens as the temperature is raised to 60 °C. Again, as in the case of the $^{11}B\{^1H\}$ spectrum, this behavior is reversible upon returning to lower temperatures.

These NMR studies were typically performed in dichloromethane, which, because of its relatively low proton affinity, is believed unlikely to significantly facilitate intermolecular proton transfer. In this system any such intermolecular proton exchange would have to occur between two already negatively charged species as there is no stoichiometric excess of H^+ present. Certainly at low temperatures (−90 °C) we have seen that the fluxional behavior of H(1) and H(*) can be arrested, suggesting that there is essentially no intermolecular exchange occurring under these conditions. However, at elevated temperatures, some type of intermolecular exchange cannot be definitively ruled out as a contributor to the clearly complex fluxional process.

Computational Characterizations. *Ab initio* calculations were employed in an effort to further understand the structure and fluxional behavior of $[B_{10}H_{11}]^-$. Computations of this type have been shown to be powerful tools for structural elucidation[16] of polyborane and related clusters.

The calculations attempted to address the following two issues: (1) determine the exact preferred location of the extra hydrogen on the anion, and (2) further understand the fluxional behavior of the cluster and support (or refute) the idea that the integral five ^{11}B NMR signal is due to magnetic equivalence and not accidental overlap of the B1 and B2−5 signals.

A previously published[7] ab initio/IGLO/NMR study of $[B_{10}H_{11}]^-$ attempted to address the location of the extra hydrogen by calculating various isomers and the corresponding ^{11}B NMR chemical shifts. Two structures were found

(16) (a) Bühl, M.; Schleyer, P. v. R. *J. Am. Chem. Soc.* **1992**, *114*, 477. (b) Bühl, M.; Gauss, J.; Hofmann, M.; Schleyer, P. v. R. *J. Am. Chem. Soc.* **1993**, *115*, 12385. (c) Onak, T.; Tran, D.; Tseng, J.; Diaz, M.; Arias, J.; Herrera, S. *J. Am. Chem. Soc.* **1993**, *115*, 9210. (d) Diaz, M.; Jaballas, J.; Arias, J.; Lee, H.; Onak, T. *J. Am. Chem. Soc.* **1996**, *118*, 4405. (e) Bausch, J. W.; Matoka, D. J.; Carroll, P. J.; Sneddon, L. G. *J. Am. Chem. Soc.* **1996**, *118*, 11423. (f) Jaballas, J.; Onak, T. *J. Organomet. Chem.* **1998**, *550*, 101. (g) Cranson, S. J.; Fox, M. A.; Greatrex, R.; Greenwood, N. N. *J. Organomet. Chem.* **1998**, *550*, 207. (h) Hofmann, M.; Fox, M. A.; Greatrex, R.; Williams R. E.; Schleyer, P. v. R. *J. Organomet. Chem.* **1998**, *550*, 331. (i) Onak, T.; Jaballas, J.; Barfield, M. *J. Am. Chem. Soc.* **1999**, *121*, 2850. (j) Shedlow, A. M.; Sneddon, L. G. *Inorg. Chem.* **1998**, *37*, 5269.

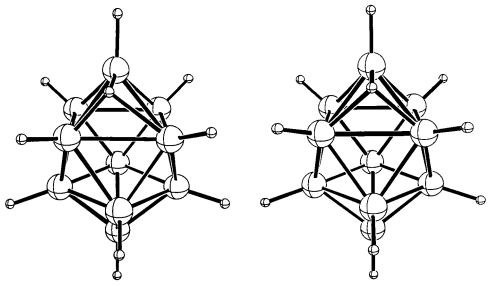

1a **1b**

Figure 8. Previously calculated HF/3-21G optimized geometries for $[B_{10}H_{11}]^-$ structures.

that roughly correspond to the structure reported here. These are shown in Figure 8.

One has the hydrogen with an asymmetrical μ-3 interaction (**1a**), while the other has the hydrogen sitting in a symmetrical μ-3 location (**1b**). Energetically they are very similar (**1b** favored by less than 1 kcal/mol at MP2/6-31G*//3-21G level of theory). The IGLO calculated (DZ//3-21G) ^{11}B NMR chemical shifts for **1a** and **1b** are given in Table 5 (second and third columns).[17] If the simpler fluxional process is occurring and there is a coincidental overlap of B1 with B2−5, then averaging the computed shifts appropriately allows the comparisons as follows (with the experimental values in parentheses).

1a: B1 −22.3 (−21.7), B2−5 −14.1 (−21.7), B6−9 −20.6 (−24.3), B10 +27.3 (+26.0)

1b: B1 −23.5 (−21.7), B2−5 −15.4 (−21.7), B6−9 −21.7 (−24.3), B10 +24.9 (+26.0)

Isomer **1b** appears to give a slightly better correlation with the experimental values, thus higher level calculations were performed[7] (DZ//MP2/6-31G) in order to improve the agreement.

1b: B1 −24.7 (−21.7), B2−5 −21.6 (−21.7), B6−9 −25.0 (−24.3), B10 +22.2 (+26.0)

The calculated value for B2−5 did improve, but perhaps at the expense of B1 and B10.

If a more complicated fluxional process is assumed whereby B1 and B2−5 are made magnetically equivalent, then comparison of the calculated shifts for **1a** and **1b** from the previous IGLO study with the experimental shifts is easily seen in Table 5. Isomer **1b** again gives better agreement with the experimental data than **1a**.

Our DFT/GIAO computational study comes to a different conclusion. The B3LYP/6-311G* optimized geometries for **1a** and **1b** are shown in Figure 9.

The structures are very similar with the extra hydrogen in **1a** located only ∼0.2 Å from a symmetrical position. Note, the bond lengths and angles calculated for **1a** (Table 6) are in good agreement with those determined from the low-temperature X-ray crystal structure (Table 2).

Table 5. Calculated ^{11}B NMR Chemical Shifts for Various $[B_{10}H_{11}]^-$ Structures

	previous study[a]			this study[b]		
atom	**1a**	**1b**[c]	**1b**[d]	expt	**1a**	**1b**
B1	−22.3	−23.5	−24.7		−25.2	+0.5
B2	−3.0	−9.8	−17.9		−10.8	−18.4
B3	−13.6	−9.8	−17.9		−21.6	−18.4
B4	−24.7	−21.0	−24.1		−25.7	−22.7
B5	−15.1	−21.0	−24.1		−17.4	−22.7
B6	−26.7	−28.7	−30.6		−26.0	−27.7
B7	−17.1	−23.0	−25.8		−20.2	−25.1
B8	−11.5	−12.2	−17.9		−17.9	−18.7
B9	−27.3	−12.2	−17.9		−28.8	−25.1
B10	+27.3	+24.9	+22.2	+26.0	+27.2	+24.6
(B1−B5)[e]	−15.7	−17.0	−22.2	−21.7	−20.1	−16.4
(B6−B9)[e]	−20.6	−21.7	−25.0	−24.3	−23.2	−24.2
(B2−B5)[e]	−14.1	−15.4	−21.6		−18.9	−20.6

[a] Reference 7. [b] GIAO B3LYP/6-311G*//B3LYP/6-311G* level. [c] IGLO DZ//3-21G level. [d] IGLO DZ//MP2/6-31G* level. [e] Averaged values.

Energetically **1a** is calculated to be just 0.1 kcal/mol more stable than the symmetrical **1b** (Table 7). This is probably well within the estimated uncertainty of the calculations. Thus, this suggests that the potential energy surface in this area is very flat. The DFT/GIAO calculated ^{11}B NMR chemical shifts for **1a** and **1b** are revealing (Table 5). Assuming the more complex fluxional process where B1 and B2−5 become magnetically equivalent, the calculated values for **1a** are in excellent agreement with the experimental values and are marginally better than those for **1b**. All three calculated shifts for **1a** are within 2 ppm of the experimental values.

If one assumes a less complex fluxional process and B1 and B2−5 coincidentally overlap, then isomer **1b** can definitely be ruled out, the reasoning being that B1 in **1b** is calculated to be at +0.5 ppm and it is unreasonable to assume that it can overlap with B2−5, which is over 20 ppm upfield. It still seems possible that **1a** could have a coincidental overlap of B1 and B2−5 since the calculated shifts (−25.2 and −18.9, respectively) are reasonably close to the experimental integral five signal at −21.7 ppm. Thus, the DFT/GIAO calculations suggest that the solution phase structure for $[B_{10}H_{11}]^-$ is the same as the solid state structure with the extra hydrogen located in an asymmetrical μ-3 fashion on the B1−B2−B3 face.

Many transition structures were reported in the previous computational study[7] to rationalize the fluxional behavior of $[B_{10}H_{11}]^-$. Recalculation of these at the higher DFT level of theory was carried out. Structure **1c** (Figure 9) represents the transition structure for the migration of the extra hydrogen in **1a** to an adjacent face in the same polar region. The barrier is calculated to be very low (0.9 kcal/mol). Such a facile process would render borons B2−5 equivalent, as well as B6−9, in apparent agreement with the experimental ^{11}B NMR ratios. A transition structure with a terminal BH_2 group, **1d**, also has a low barrier (5.7 kcal/mol) and connects **1b** with another **1b** with an extra hydrogen now on the opposite face in the same polar region.

(17) In the previous computational study (ref 7), apparently the authors reversed the integrations of the two upfield boron resonances by mistake. The intensities are in fact 1:5:4 going from low-field to high-field. Because these two resonances are so close, it does not substantially alter the arguments made in their paper. We have corrected this data in Table 5.

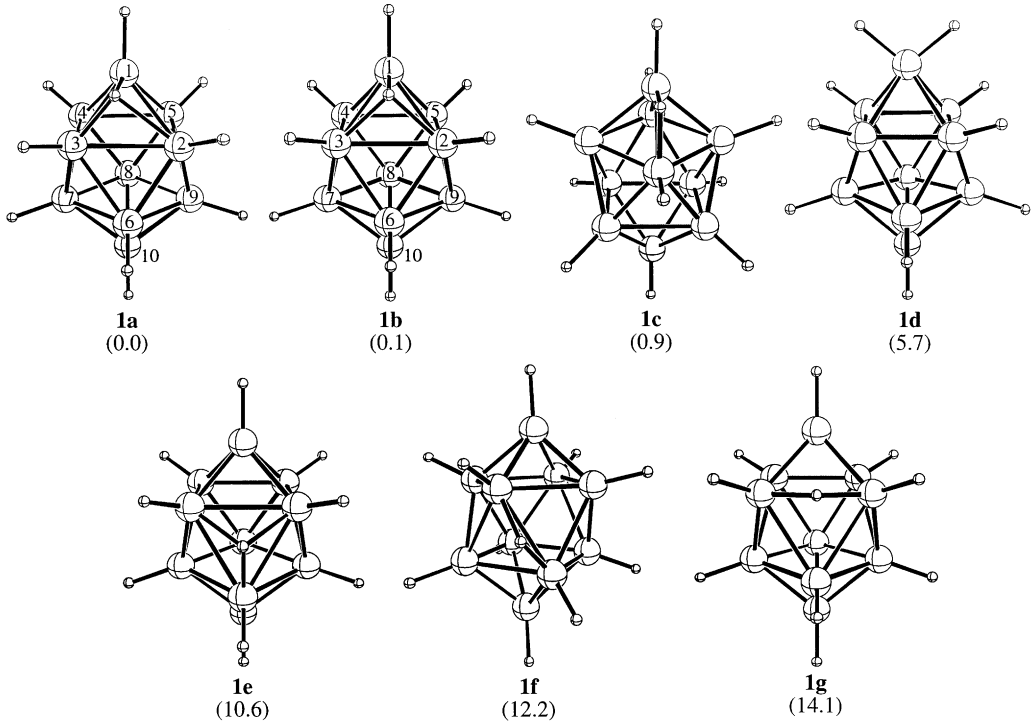

Figure 9. DFT optimized geometries for $[B_{10}H_{11}]^-$ structures **1a**−**g**, with the relative energies shown in parentheses.

Table 6. Selected Interatomic Distances (Å) and Angles (deg) from the DFT Calculated Structure **1a**

B1−B2	1.843	B4−B8	1.812	B3−B1−B2	68.6
B1−B3	1.799	B5−B8	1.816	B3−B1−B4	61.8
B1−B4	1.714	B5−B9	1.800	B2−B1−B5	59.8
B1−B5	1.712	B6−B7	1.890	B4−B1−B5	66.4
B2−B3	2.054	B6−B9	1.852	B3−B2−B1	54.7
B2−B5	1.775	B6−B10	1.716	B2−B3−B1	56.7
B2−B6	1.809	B7−B8	1.807	B4−B3−B1	56.8
B2−B9	1.787	B7−B10	1.682	B2−B5−B1	63.8
B3−B4	1.805	B8−B9	1.827	B3−B6−B2	68.4
B3−B6	1.845	B9−B10	1.686	B3−B2−B6	56.6
B3−B7	1.825	B1−Hb	1.282	B2−B3−B6	54.0
B4−B5	1.877	B2−Hb	1.688	B9−B2−B6	62.0
B4−B7	1.788	B3−Hb	1.422	B8−B10−B7	64.2
				B1−Hb−B3	83.3
				B1−Hb−B2	75.3
				B3−Hb−B2	82.2

Table 7. Absolute (−au) and Relative (kcal/mol) Energies of $[B_{10}H_{11}]^-$ Isomers Calculated in This Study

structure	sym	B3LYP/6-311G*// B3LYP/6-311G*	ZPE (NAV)[a]	E_{rel}[b]
1a	C_1	255.32946	89.78 (0)	0.0
1b	C_s	255.32942	89.85 (0)	0.1
1c	C_s	255.32864	90.17 (1)	0.9
1d	C_{2v}	255.31958	89.31 (1)	5.7
1e	C_s	255.31245	89.68 (0)	10.6
1f	C_2	255.30913	89.12 (1)	12.1
1g	C	255.30562	88.91 (1)	14.1
1h	C_s	255.28680	88.35 (1)	25.3
1i	C_1	255.28619	89.09 (1)	26.5
1j	C_s	255.25199	88.73 (1)	47.6

[a] Zero point energy (kcal/mol) and number of imaginary frequencies in parentheses. [b] Relative energy at the B3LYP/6-311G*//B3LYP/6-311G* + ZPE level; the zero point energies are unscaled.

A higher energy $[B_{10}H_{11}]^-$ intermediate, **1e**, has the extra hydrogen symmetrically located on the B2−B3−B6 face. It is calculated to be 10.6 kcal/mol higher in energy than **1a**. This structure is an intermediate on the pathway for migration of the extra hydrogen from one polar region to the other. The transition structure that connects **1b** and **1e** is **1g**. The barrier for this process is calculated to be 14.1 kcal/mol. Structure **1f** is a transition state that connects **1e** with an equivalent **1e** with the extra hydrogen now on an adjacent face in the same "belt" region. The barrier for this degenerate rearrangement is calculated to be quite small (1.5 kcal/mol).

Thus, the calculations suggest a fairly flat potential energy surface for migration of the extra hydrogen all over the cluster, with the largest barrier being 14.1 kcal/mol. At sufficiently high temperatures it should be possible to allow observance of just two signals in the $^{11}B\{^1H\}$ NMR spectrum in a 4:1 ratio indicating that both apical borons and the eight belt borons have become equivalent on the NMR time scale. However, the high-temperature $^{11}B\{^1H\}$ NMR data (+30 to +60 °C) of $[B_{10}H_{11}]^-$ show (Figure 4) that above 50 °C the low-field signal B10 is broadened into the baseline, and the two higher field signals coalesce into a single peak centered at the two high-field room temperature signals. This result suggests that the dynamic behavior of $[B_{10}H_{11}]^-$ could be more complicated than that just involving facile proton migration around the cluster.[18]

The $^{11}B\{^1H\}-^{11}B\{^1H\}$ NOESY/EXSY experiment (Figure 5) on $[B_{10}H_{11}]^-$ showed cross peaks with the same phase and that are relatively large with respect to the on-diagonal peaks. This suggests that exchange between all cage vertices is occurring to some extent, even at room temperature. Cage

(18) It is possible, for reasons that are yet to be understood, that the high-temperature ^{11}B NMR spectrum of $[B_{10}H_{11}]^-$ does represent a 4:1 ratio of signals expected if there is facile migration of the extra hydrogen around the cluster, but the integral one signal (representing B1 and B10) is extremely broad. The calculations predict this signal to be at +1.0 ppm (with the B2−B9 signal at −23.0 ppm).

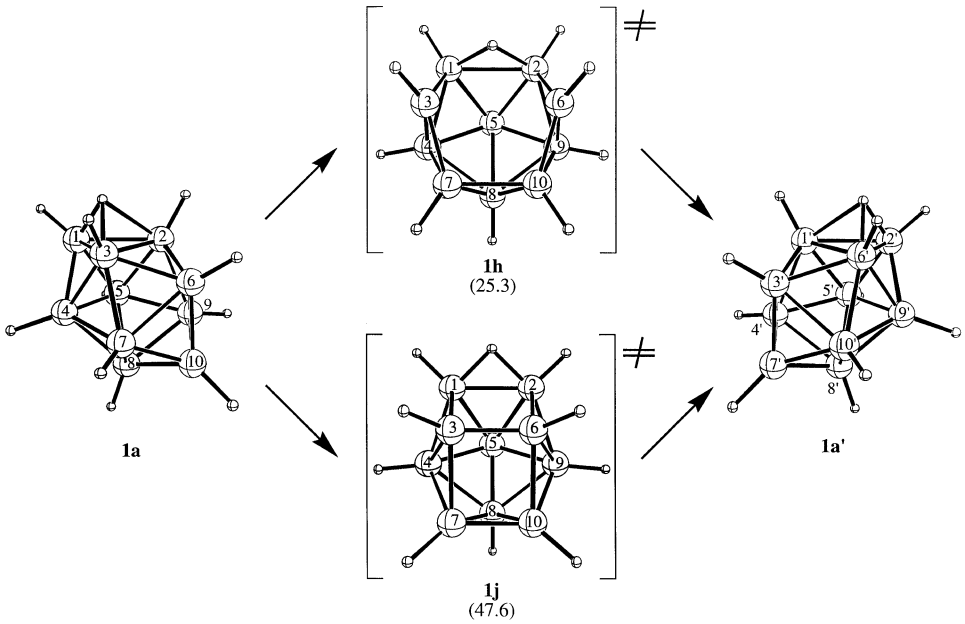

Figure 10. Two possible degenerate rearrangement pathways for **1a**.

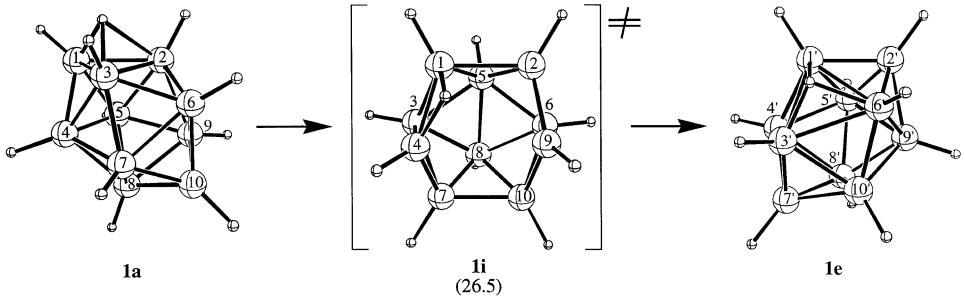

Figure 11. Cage rearrangement pathway converting **1a** to **1e**.

rearrangements are fairly common in polyhedral boranes; thus it would not be surprising to find the same in this system. Employing the QST2 option within Gaussian 94, three different transition structures have been located involving cage rearrangement.

A transition structure (**1h**) corresponding to a degenerate cage rearrangement of **1a** is shown in Figure 10. It has a six-membered open face with the extra hydrogen bridging two adjacent four-coordinated borons on the open face. This transition structure is calculated to be 25.3 kcal/mol higher in energy than **1a**. This process converts the two apical borons into belt borons and vice versa. This rearrangement may have a low enough barrier to account for the NOESY/EXSY data. A structure (**1j**) was also found that connects the same two structures (Figure 10), but its barrier is much higher (47.6 kcal/mol).

Another transition structure (**1i**) involving cage rearrangement was found and connects **1a** and **1e**. This is shown in Figure 11. It also contains a six-membered open face like **1h**, but it has the extra hydrogen bridging adjacent three- and four-coordinated borons on the open face. The barrier for this cage rearrangement is calculated to be 26.5 kcal/mol. This process would also convert two apical borons to belt borons and vice versa.

These cage rearrangements may explain the NOESY/EXSY NMR data. However, none of them are able to answer the question as to whether the integral five signal in the ^{11}B-{^{1}H} NMR spectrum is due to some facile rearrangement process that makes B1 and B2−5 magnetically equivalent on the NMR time scale, or whether it is simply a coincidental overlap. Numerous attempts were made to find other transition states involving more facile cage rearrangements that would make B1−5 equivalent, but no others were found.

In previous studies showing fluxionality in 10-vertex closo species,[26,27] it has been suggested that the cluster rearrange-

(19) Otwinowsky, Z.; Minor, W. Processing of X-ray Diffraction Data Collected in Oscillation Mode. In *Methods in Enzymology, Vol. 276: Macromolecular Crystallography, Part A*; Carter, C. W., Jr., Sweet, R. M., Eds.; Academic Press: New York, 1997; pp 307−326.
(20) SHELXTL (version 5.10), Bruker Analytical X-ray Systems, 1997.
(21) Frisch, M. J.; Trucks, G. W.; Schlegel, H. B.; Gill, P. M. W.; Johnson, B. G.; Robb, M. A.; Cheeseman, J. R.; Keith, T.; Peterson, G. A.; Montgomery, J. A.; Raghavachari, K.; Al-Laham, M. A.; Zakrzewski, V. G.; Ortiz, J. V.; Foresman, J. B.; Cioslowski, J.; Stefanov, B. B.; Nanayakkara, A.; Challacombe, M.; Peng, C. Y.; Ayala, P. Y.; Chen, W.; Wong, M. W.; Andres, J. L.; Replogle, E. S.; Gomperts, R.; Martin, R. L.; Fox, D. J.; Binkley, J. S.; Defrees, D. J.; Baker, J.; Stewart, J. P.; Head-Gordon, M.; Gonzalez, C.; Pople, J. A. *Gaussian 94*, revision E.2; Gaussian, Inc.: Pittsburgh, PA, 1995.
(22) Tebben, A. J. Master's Thesis, Villanova University, 1997.
(23) Maerker, C.; Schleyer, P. v. R.; Salahub, D. R.; Malkina, O. L.; Malkin, V. G., private communication.
(24) Pena, C.; Schlegel, H. B. *Isr. J. Chem.* **1993**, *33*, 449.

ments might occur via a series of successive diamond−square−diamond (DSD) transformations (a suggestion also made by a referee of this paper). In the case of the *closo*-$[Sn_9M(CO)_3]^{4-}$ clusters[26] (where M = Cr, Mo, and W), the net effect of these rearrangements is the equilibration of structures containing η^4 (M in apical position) and η^5 (with M equatorial) arrangements at one end of the cluster. While this fluxionality of only one part of the closo cluster is clearly similar to that observed in our study at low temperature, we were unable to identify any suitably low energy pathway of this type for the $[B_{10}H_{11}]^-$ system. As discussed above, the initial pathway we identified for the degenerate transformation of **1a** to **1a′** involved transition state **1j**, which can be viewed as two simultaneous DSD rearrangements. The barrier to this process was somewhat high (47.6 kcal/mol), and so we searched for other possible pathways. The only other transition state we located was **1h**, which has a much lower energy barrier (25.3 kcal/mol). In the case[27] of the metallacarboranes [2-(η^6-C_6Me_6)-*closo*-2,1,6-$RuC_2B_7H_9$] and [2-(η^5-C_5Me_5)-*closo*-2,1,6-$RhC_2B_7H_9$], fluxionality of selected cluster vertices is also suggested to occur via two DSD processes, although the authors do not specify whether these are thought to occur sequentially or in concert.

Experimental Section

General Comments. All manipulations were performed using standard high vacuum line techniques or in a drybox under N_2. CH_2Cl_2 and CH_3CN were dried over P_2O_5. Previously dried solvents were freshly distilled into the reaction flasks prior to use. CF_3COOH was obtained from Aldrich Chemical Co. and used as received in a glovebag. $[Ph_4P]_2[B_{10}H_{10}]$, $[PPh_3(benzyl)]_2[B_{10}H_{10}]$, and $[PPh_3(Et)]_2[B_{10}H_{10}]$ were prepared from metathesis reactions between THF solutions of $Na_2[B_{10}H_{10}]$ and CH_2Cl_2 solutions of $[Ph_4P]Br$, $[PPh_3(benzyl)]Cl$, and $[PPh_3(Et)]Cl$, respectively. All IR spectra were recorded with 2-cm^{-1} resolution using a Mattson-Polaris FT-IR spectrometer. ^{11}B NMR spectra [δ (Et_2OBF_3) = 0.00 ppm, positive shifts to high frequency] were obtained on either a Bruker DRX-250, DRX-500, or DMX-300 NMR spectrometer operating at 80.2, 160.1, and 96.3 MHz, respectively. ^1H NMR spectra [δ ($Si(CH_3)_4$) = 0.00 ppm] were obtained on a Bruker DMX-300 spectrometer operating at 300.1 MHz.

$[Ph_4P][B_{10}H_{11}]$. In a typical reaction, $[Ph_4P]_2[B_{10}H_{10}]$ (0.610 g, 0.766 mmol) was dissolved in CH_3CN (20 mL) and CF_3CO_2H (1.8 mL) was injected. The clear solution was stirred at room temperature for 2 h and then reduced in volume in vacuo to approximately 5 mL. Slow cooling to 0 °C afforded a white crystalline product, which was collected by filtration, $[Ph_4P][B_{10}H_{11}]$ (0.311 g, 0.678 mmol), in 88.5% yield.

IR (KBr): 3078 (w); 3060 (w); 2541 (s); 2488 (s); 1586 (w); 1483 (m); 1435 (s); 1338 (w); 1313 (w); 1183 (w); 1116 (w); 1107 (s); 1028 (w); 995 (m); 758 (m); 746 (w); 722 (s); 687 (s); 526 (s) cm^{-1}. ^{11}B NMR (CD_2Cl_2, 23 °C): +26.0 ppm (d) [1B], J_{BH} 159 Hz; −21.7 ppm (d) [5B], J_{BH} 148 Hz; −24.3 ppm (d) [4B], J_{BH} 145 Hz. ^1H NMR (CD_2Cl_2, 23 °C): 7.47−7.82 ppm (mult, Ph).

$[PPh_3(benzyl)][B_{10}H_{11}]$ and $[PPh_3(Et)][B_{10}H_{11}]$ were prepared in high yield from $[PPh_3(benzyl)]_2[B_{10}H_{10}]$ and $[PPh_3(Et)]_2[B_{10}H_{10}]$ in identical procedures.

$[PPh_3(benzyl)][B_{10}H_{11}]$. IR (KBr): 3078 (w); 3055 (w);2948 (w); 2905 (w); 2544 (m, sh); 2512 (s); 2480 (s); 1587 (w); 1496 (w); 1483 (w); 1456 (w); 1438(s); 1332 (w); 1317 (w); 1187 (w); 1112 (m); 997 (m); 841 (w); 835 (w); 783 (w); 748 (m); 723 (w); 716 (m); 688 (s); 582 (m); 509 (s); 487 (m) cm^{-1}. ^{11}B NMR (CD_2Cl_2, 23 °C): +25.0 ppm (d) [1B], J_{BH} 159 Hz; −22.7 ppm (d) [5B], J_{BH} 148 Hz; −25.2 ppm (d) [4B], J_{BH} 145 Hz. ^1H NMR (CD_2Cl_2, 23 °C): 6.75−7.76 ppm (mult, Ph), 4.43 (d, Ph−CH_2−P).

$[Ph_3P(Et)][B_{10}H_{11}]$. IR (KBr): 3058 (w); 2978 (w); 2940 (w); 2910 (w); 254 (s, sh); 2476 (s); 1587 (w); 1485 (w); 1438 (s); 1404 (w); 1341 (w); 1320 (w); 1189 (w); 1161 (w); 1114 (m); 996 (m); 822 (w); 753 (m); 740 (s); 722 (m); 692 (m); 530 (s); 509 (m); 486 (m); 452 (w) cm^{-1}. ^{11}B NMR (CD_2Cl_2, 23 °C): +25.0 ppm (d) [1B], J_{BH} 159 Hz; −22.7 ppm (d) [5B], J_{BH} 148 Hz; −25.2 ppm (d) [4B], J_{BH} 145 Hz. ^1H NMR (CD_2Cl_2, 23 °C): 7.44−7.94 ppm (mult, Ph), 3.14 (d of q, CH_3-CH_2-P), 1.25 (d of t, CH_3-CH_2-P).

Inversion Recovery Experiments on $[Ph_4P][B_{10}H_{11}]$. All experiments were caried out on a Bruker DRX-500 spectrometer. The inversion recovery pulse sequence (supplied by Bruker) is shown below.[13]

B11: d1−p2−vd−p1−acq

vd	variable delay
d1	recycle delay
p1	90° B11 pulse
p2	180° B11 pulse

The variable delays used were 0.5, 0.2, 0.1, 0.05, 0.02, 0.01, and 0.005 s. The boron resonance frequency is 160.461 MHz. Temperature was 27 °C for all experiments.

NOESY/EXSY Experiments on $[Ph_4P][B_{10}H_{11}]$ and $[Ph_4P]_2[B_{10}H_{10}]$. All NOESY/EXSY experiments were caried out on a Bruker DRX-500 spectrometer. The gradient EXSY/NOESY sequence used was phase sensitive using TPPI. The pulse sequence (supplied by Bruker) is shown below.[14,15]

B11: d1−p1−d0−p1−mix−p2−mix−p1−acq

Z-grad: gp1 −gp1

d0	incremental delay
d1	recycle delay
mix	mixing time
p1	90° B11 pulse
p2	180° B11 pulse
gp1	gradient pulse

The boron resonance frequency is 160.461 MHz. Mixing times used were 10 ms or 50 ms. Temperature was 27 °C for all experiments.

X-ray Structure Determination. Single-crystal X-ray diffraction data were collected on an Enraf-Nonius KappaCCD diffraction system, employing graphite-monochromated Mo Kα radiation, λ = 0.71073 Å. A single crystal of $[PPh_3(benzyl)][B_{10}H_{11}]$ was mounted on a glass fiber coated with Fomblin oil (a perfluoropolyether). Data were collected at −123 °C. Unit cell parameters were obtained by indexing the peaks in the first 10 frames and refined using the whole data set. All frames were integrated and corrected for Lorentz and polarization effects using DENZO.[19] The structure was solved in the monoclinic space group $P2_1/c$ by direct methods and refined using SHELXTL (difference electron density calculations, full least-squares refinement).[20]

Additional data sets were collected in the same manner at −93, −63, −38, −3, and 24 °C using the same crystal.

Computational Studies. All *ab initio* calculations were performed employing the Gaussian 94 program.[21] The geometries were

(25) Gonzalez, C.; Schlegel, H. B. *J. Phys. Chem.* **1990**, *94*, 5523.
(26) Kesanli, B.; Fettinger, J.; Eichhorn, B. *Chem. Eur. J.* **2001**, *7*, 5277.
(27) Bown, M.; Jelínek, T.; Štíbr, B.; Heřmánek, S.; Fontaine, X. L. R.; Greenwood, N. N.; Kennedy, J. D.; Thornton-Pett, M. *J. Chem. Soc., Chem. Commun.* **1988**, 974.

fully optimized at the DFT B3LYP/6-311G* level within the specified symmetry constraints on Linux-based PC computers. A vibrational frequency analysis was carried out on each optimized geometry to characterize the nature of the stationary point. The NMR chemical shifts were calculated at the GIAO B3LYP/6-311G* level, referenced to Et_2OBF_3 using an absolute shielding constant of 102.24, and corrected[22] using a method analogous to the one described by Schleyer for ^{13}C NMR shifts.[23] The ^{1}H NMR chemical shifts are referenced to tetramethylsilane using an absolute shielding constant of 32.31. Transition states were initially located at a lower level of theory employing the STQN methods[24] (invoked with the QST2 option within Gaussian 94), each connected intended minimum was verified by doing a reaction path calculation[25] (using the IRC keyword), and then the transition states were optimized at higher levels of theory using the OPT=TS option.

Supporting Information Available: Crystallographic information in CIF format. This material is available free of charge via the Internet at http://pubs.acs.org.

IC020540S